Kalala *et al.*
*Journal of Engineering and Applied Science* (2024) 71:119
https://doi.org/10.1186/s44147-024-00452-4

Journal of Engineering and Applied Science

RESEARCH Open Access

# Numerical analysis of a protective coating for mining industry feed chute

Michael Kalala[1], Patrick Kisula[1], Innocent Muheme[2] and Lagouge Tartibu[3*]

*Correspondence:
ltartibu@uj.ac.za

[1] Department of Electromechanical Engineering, University of Lubumbashi, Lubumbashi, Democratic Republic of Congo
[2] Department of Electrical and Electronic Engineering Science, University of Johannesburg, Johannesburg, South Africa
[3] Department of Mechanical and Industrial Engineering Technology, University of Johannesburg, Johannesburg, South Africa

## Abstract

The selection of materials for the protective coating of a crusher's feed chute significantly influences the mean time between failures (MTBF) and operational costs associated with the mass production of sulfuric acid at MMG/Kinsevere. Neglecting the condition of the protective coating can pose a serious challenge to production efficiency and result in increased downtime. This study focuses on enhancing industrial productivity in Sulfuric Acid production with minimal maintenance. The investigation explores the quality and type of materials used for the protective coating of the feed chute in the mining industry, particularly at MMG/Kinsevere, utilizing Ansys Fluent and SOLIDWORKS Software for analysis. The paper proposes a Ceramic protective liner for the crusher feed chute due to its superior resistance to erosion compared to other liners. Different feed chute models, constructed with materials like halogenated butyl rubber, 316 stainless steel, and ceramic, underwent analysis. The evaluation of the potential impact on the mean time between failures (MTBF) for different materials used in a protective coating, considering the rate of erosion through computational fluid dynamics (CFD) with ANSYS FLUENT software, is a central aspect of this study. The detailed modeling and simulation reveal that the ceramic material exhibits the most favorable protective coating characteristics, with an erosion rate density of 06.636753 kg/m$^2$s, outperforming halogenated butyl rubber (3.326576 kg/m$^2$s) and 316 stainless steel (2.186633 kg/m$^2$s). The simulation yielded results corresponding to flow rates of 284.19 kg/s for the solid phase and 123.14 kg/s for the liquid phase.

**Keywords:** Protective coating, Crusher, Numerical analysis, Maintenance

## Introduction

In the realm of engineering materials, the selection process is critical, especially when considering the strength and erosion resistance of elements in construction. This is particularly pertinent in the design of protective coatings for crusher feed chutes, where the use of innovative, high-density materials is essential to ensure structural integrity and longevity.

The grinding circuit plays a crucial role in particle size reduction, a process necessary for the effective dissolution of materials in sulfuric acid. This circuit, which involves a semi-autogenous mill (SAG MILL) and a wet grinding machine, is well-documented by SPW (10) and Suhr et al. [12]. Despite the importance of this stage, the crusher's feed

chute is subject to premature wear, leading to frequent maintenance shutdowns. These interruptions are costly and highlight the need for a more durable protective coating.

Maintenance typically entails replacing the existing protective coating, which is presently made of halogenated butyl rubber. The recurring nature of these operations underscores the importance of enhancing the mean time between failures (MTBF) of the chute. Research into coating strength and damage mechanisms, such as the work by Noguchi [6] and Xu et al. [15], has provided valuable insights into the development of more resilient materials.

This paper aims to enhance this knowledge base by introducing a novel protective coating for the crusher's feed chute. The methodology is driven by computational fluid dynamics (CFD) analyses, drawing insights from influential researchers like Franklin (4). Franklin advocates for employing the Reynolds averaged Navier–Stokes (RANS) approach, highlighting its balanced accuracy and computational efficiency. The study employs Ansys Fluent simulations to evaluate the performance of new materials and designs, with the goal of enhancing the operational efficiency of mining activities. This challenge is underscored by Sánchez and Hartlieb [9], who highlight the escalating operational and environmental pressures confronting the mining industry.

The methodology of this study begins with the development of an Ansys Fluent geometry simulation to accurately replicate the crushing circuit. Various designs for the protective coating of the feed chute are explored through simulations, aiming to achieve a more uniform feed distribution. Following this, the optimal design is implemented during the construction and installation phases to seamlessly integrate the new protective coating feed chute onto the crusher. This initiative is anticipated to enhance the operational efficiency of mining activities linked with the crusher at MMG/Kinsevere. It is poised to contribute to the industry's endeavors in addressing challenges like declining ore grades and increasing environmental and social awareness.

Figure 1 illustrates the fragmentation process, including crushing to grinding, and the different flows fed into the crusher through the chute. Figures 2 and 3 illustrate degraded coating.

## Methods

### Model geometry

Three distinct flows—ores, raffinate, and pulp—were meticulously chosen for in-depth examination to assess their impact on the protective coating of the feed chute. The analysis involved scrutinizing the results of numerical simulations conducted in ANSYS FLUENT software. ANSYS is a user-friendly software offering a plethora of options for conducting 2D and 3D simulations on geometries of varying complexity. It accommodates both fixed and adaptive meshes and supports various physical models, including those for two-phase and turbulent flows. The software's accessibility and versatility were key factors in opting for ANSYS to execute the simulations. Simulations in ANSYS are performed through the Ansys Workbench interface, a valuable tool for managing single or multiple simulations, especially in fluid mechanics. The Ansys Fluent analysis system involves five major steps: geometry creation, mesh generation, solver configuration, numerical resolution, and the display and visualization of results.

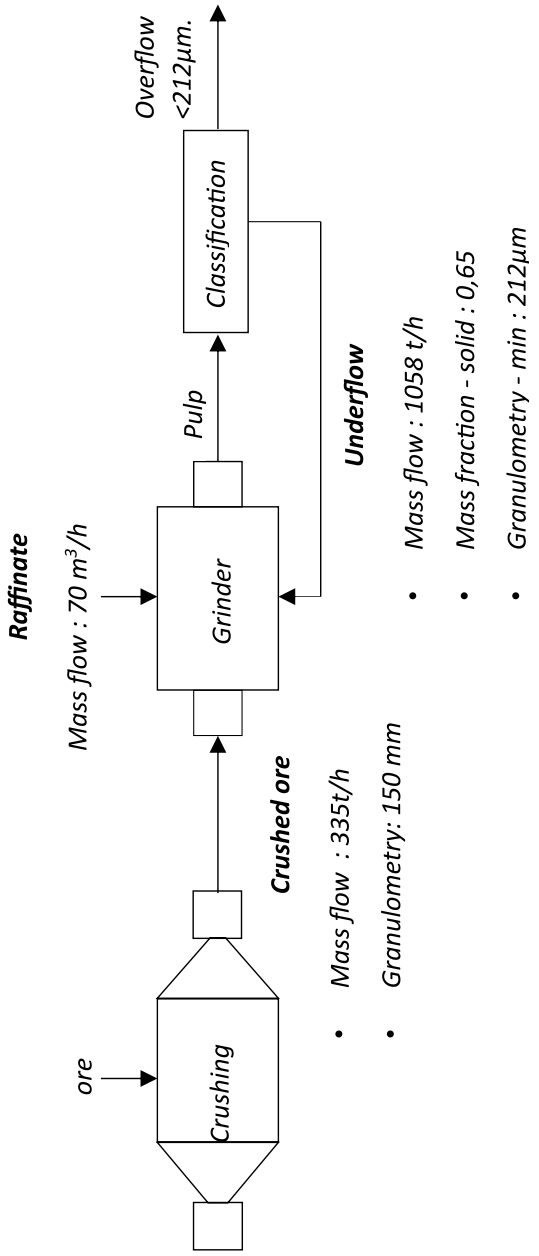


**Fig. 1** Flow identification fed SAG mill

**Fig. 2** Worn-out coating state

**Fig. 3** Protective coating degraded

In both structural and fluid mechanics simulations, the first step is to generate the geometry in either 2D or 3D. This can be accomplished using software integrated into the calculation code or via computer-aided design (CAD) software. In the latter case, the geometry is typically imported in a format compatible with the simulation software, with STEP or IGES formats being the most commonly used [1]. For this project, the trunking geometry was crafted using SOLIDWORKS 2018 software and then exported in IGES format.

### Generation of the mesh and definition of the boundary conditions

Mesh generation is a crucial step wherein a given geometry is discretized into multiple elements [11]. In this phase, the objective was to create a mesh for the geometry, delineating key boundaries such as the inlet, outlet, and walls. The meshing process was executed using the Ansys Fluent Mesher, which carries out meshing operations through a series of steps: importing the geometry for meshing, generating a mesh for the solid domain, specifying geometry limits, and generating the mesh for the fluid domain. The imported geometry underwent meshing, as illustrated in Figs. 4 and 5, following the dimensions specified in Table 1.

The delineation of limits involved specifying the fluid inlet, outlet, and coating walls, as depicted in Fig. 6. Subsequently, upon defining these limits, the mesh for the fluid domain was generated (refer to Fig. 7), with corresponding properties outlined in Table 2.

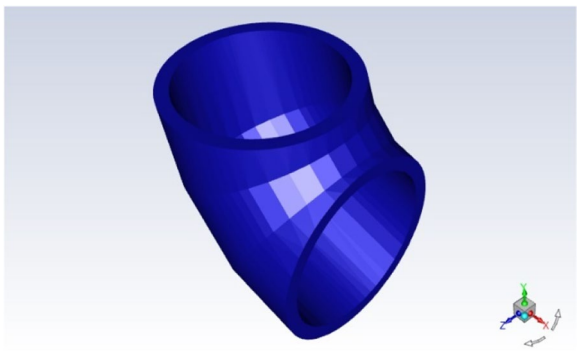

**Fig. 4** Chute geometry

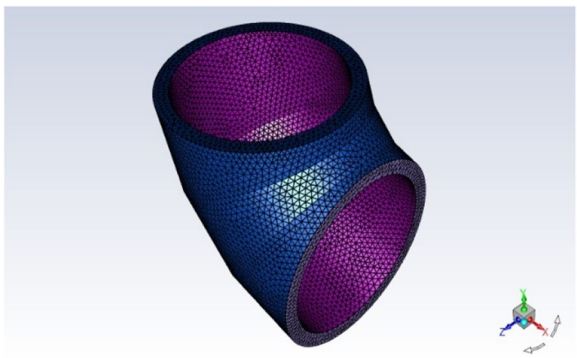

**Fig. 5** Geometry mesh

**Table 1** Mesh specifications

| Title | Value |
|---|---|
| Minimum size | 1.6 mm |
| Maximum size | 41 mm |
| Growth rate | 1.2 |

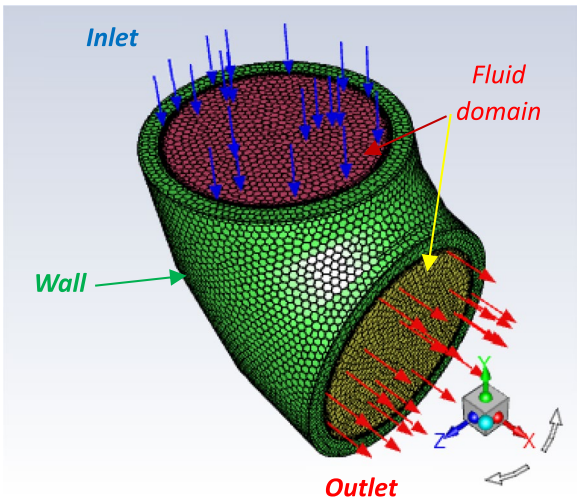


**Fig. 6** Limits of the chute

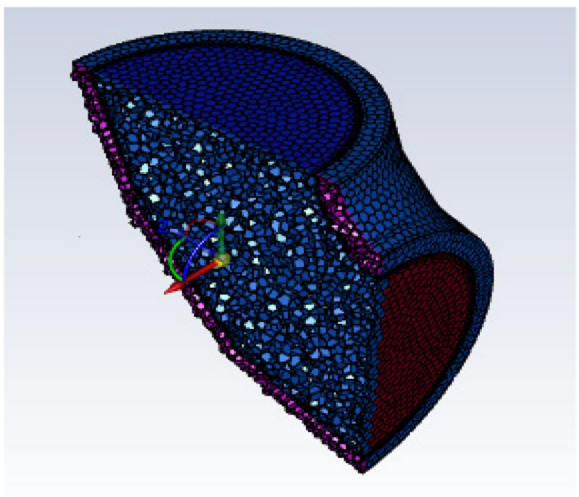

**Fig. 7** Mesh of the fluid dominance

**Table 2** Generation of the fluid domain mesh

| Title | Value |
|---|---|
| Mesh | Polyhedral |
| Growth rate | 1.2 |
| Maximum cell size | 57 mm |

### Modeling with Ansys Fluent

The Ansys Fluent solver was set up following distinct steps, as illustrated in Fig. 8.

Given that the flow is incompressible and considered steady, the solver types "pressure-based" and "steady" were selected, respectively. Ansys Fluent provides four models: Volume of Fluid or miscible phases (VOF), Mixture, Wet Steam, and Eulerian. The first two models are designed for homogeneous flows, while the last two are suitable for heterogeneous


**Fig. 8** Solver configurations

flows. Considering that the flow in the feed chute is considered heterogeneous, the Eulerian model, combined with the Lagrangian approach for resolving the solid phase, was chosen.

The flows within the feed chute exhibit disordered and non-parallel streamlines, indicating turbulent behavior. Therefore, the flow was configured to account for turbulence. The material assignment involves defining the substances present in the flows. In this study, the assignment designates raffinate as the primary or liquid phase and copper as the secondary or discrete phase. At the entrance of the chute, "velocity inlet" type boundary conditions were selected. Ansys Fluent Software provides various methods to define material velocity direction, and, for this study, the direction chosen was perpendicular to the surface of the chute inlet. The boundary conditions considered at the entrance of the chute are detailed in Table 3. These values were gathered from the operating conditions at MMG/Kinsevere.

In this study, the Oka erosion model was used to predict the rate of erosion in the chute [7, 8]. This model considers several influencing parameters, some of which are readily available in the literature. In addition, this model is a predictive expression in terms of the quality and quantity of the erosion rate applicable irrespective of velocity, impact angle, type of material eroded, and size of eroding material.

This model is given by the Eq. (1):

$$E(\theta) = g(\theta)E(90^{\circ}) \tag{1}$$

With.

$E(\theta)[mm^3/kg]$: is the erosion rate for any impact angle θ.

$E(90^{\circ})[mm^3/kg]$: is the erosion rate when θ is normal to the impact surface.

$g(\theta)$: is a function that considers the dependence of erosion on θ, and the hardness of the eroded material expressed in GPa.

The function g(θ) is given by the mathematical Eq. (3):

$$g(\theta) = (\sin\theta)^{n_1}(\sin\theta)^{n_1}n_1(1 + Hv(1 - \sin\theta))^{n_2} \tag{2}$$

where $n_1$ and $n_2$ are empirical constants determined via the hardness of the eroded material and other impact conditions such as the properties of the eroding material. These constants are given in Eqs. (3) and (4).

$$n_1 = 0.71(Hv)^{0.14} \tag{3}$$

**Table 3** Boundary conditions at the chute inlet

| **Primary phase** | |
|---|---|
| **Raffinate mass flow** | **70 [$m^3$/h] or 20.22 [kg/s]** |
| Mass flow solution circulating load | 370.51 [t/h] or 102.9194 [kg/s] |
| Total fluid mass flow supplied | 123.14 [kg/s] |
| Discrete phase | |
| Solid mass flow from the crusher | 335 [t/h] or 93.06 [kg/s] |
| Solid mass flow circulating load | 688.09 [t/h] or 191.14 [kg/s] |
| Total solid-fed mass flow | 1023 [t/h] or 284.19 [kg/s] |

**Table 4** Boundary conditions of the wall

| Title | Value or choice |
|---|---|
| Solid phase normal reflection coefficient | 1.5 |
| Solid phase tangent reflection coefficient | 0.61 |
| Erosion model | Oka model |

**Table 5** Parameters of the Oka model depending on the material

| | Rubber | Stainless steel 316 | Ceramic |
|---|---|---|---|
| $n_1$ | 0.747910911 | 0.791339258 | 0.920912723 |
| $n_2$ | 1.692486914 | 1.158614854 | 0.418566719 |
| $k_2$ | 2.332704999 | 2.368717703 | 2.468245996 |
| Hv | 1.45 GPa | 2.17 GPa | 6.41 GPa |
| $E_{90}$ | 0.328026792 $mm^3/kg$ | 0.283591853 $mm^3/kg$ | 0.190372948 $mm^3/kg$ |

$$n_2 = 2.4(\mathrm{Hv})^{-0.94} \tag{4}$$

The $E(\theta)$ function is given by the following equation:

$$E_{90} = 60(\mathrm{Hv})^{-0.12}\left(\frac{d}{d_{ref}}\right)^{0.019}\left(\frac{v}{v_{ref}}\right)^{k_2} \tag{5}$$

where.

$v$: represents impact velocity.

$d$: represents particle diameter.

$d_{ref}$: represents the wall boundary conditions that have been specified (refer to Table 4).

These conditions primarily involve determining the wear model (Oka) to be applied and defining the necessary parameters for its implementation across various case studies (refer to Table 5). Multiple case studies were conducted by varying the wall material, representing the coating of the chute. Three materials were examined: halogenated butyl rubber, the current coating used to safeguard the feed chute of the MMG/Kinsevere mill; 316 stainless steel, commonly employed in transporting acidic materials through pipes; and ceramics, known for its superior abrasion hardness, increasingly utilized in the mining industry, especially for safeguarding hydrocyclones. Tables 4 and 5 provide insights into some wall boundary conditions and parameters of the selected Oka model based on the material type.

Prior to commencing the computation, initializing the values of various variables in the problem, such as velocity, pressure, temperature, and turbulence equations, is crucial. In this study, hybrid initialization was adopted. This method involves the software initializing the solutions by considering all the boundaries of the domain.

## Results and discussions

The grid convergence test was performed to analyze the effect of the mesh size on the rate of erosion density. The mesh size was adjusted between 0.03 and 0.05 mm. Figure 12a–c shows the results corresponding to stainless steel, ceramic, and rubber, respectively. These convergence plots show the convergence of the simulations.

**Table 6** Comparative table of densities of erosion rates according to the turbulence model

| Turbulence model | Erosion rate density |
|---|---|
| k-ξ Standard | 0.66357 |
| k-ξ RNG | 0.67458 |
| Reynold stress | 0.67610 |
| k-ω SST | 0.6637 |
| k-ω Standard | 0.66367 |
| k-ω GEKO | 0.66120 |
| k-ω BSL | 0.66118 |

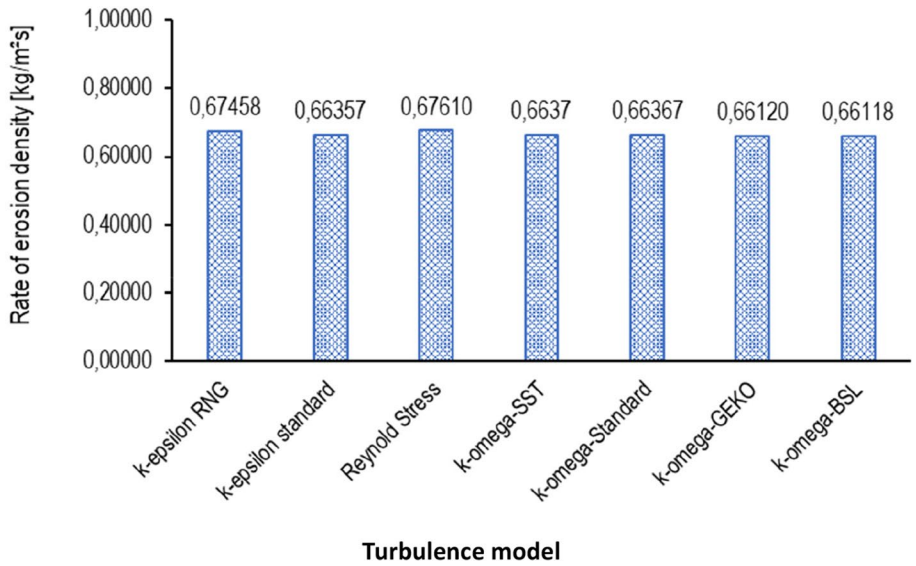


**Fig. 9** Dependence of erosion rate densities on the turbulence model

The outcomes of the residual convergence test demonstrated convergence levels up to $10^{-5}$ for continuity and $10^{-6}$ for all other variables (velocity along $x$, velocity along $y$, velocity along $z$, kinetic energy $k$, and the specific rate of dissipation $\Omega$), reaching this convergence at iteration number 530.

Table 6, depicted in Fig. 9, displays the outcomes concerning the influence of the turbulence model selection on the density of the erosion rate. An examination of Table 6 and Fig. 10 reveals, for this specific case study, the insignificance of the density of the erosion rate in relation to the chosen turbulence model. The analysis indicates that the variations between the different models are minimal, up to the closest ten thousandth. Consequently, regardless of the model employed, the obtained results would not have exhibited significant differences.

The simulation results indicate that the area with the highest density of the erosion rate aligns with the observed region on the currently used chute. Figure 11 visually represents this correlation.

Furthermore, the simulations reveal that the high-density zone of the erosion rate is consistent across different materials. Figures 12, 13, and 14 illustrate that the area with

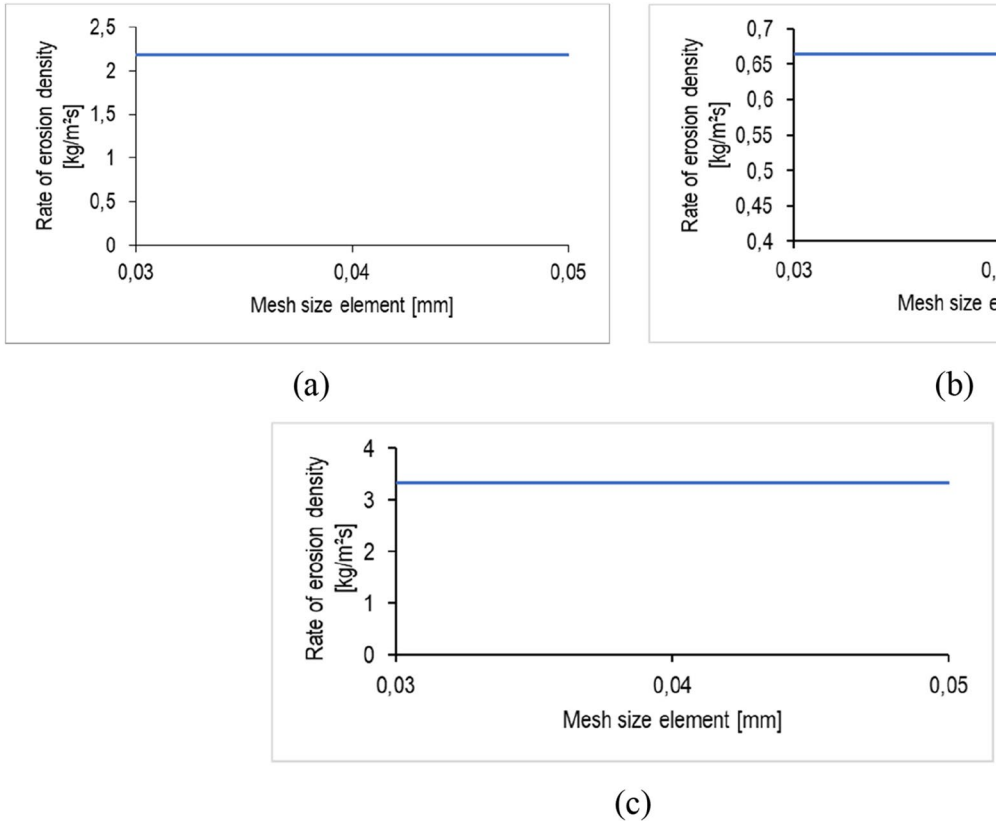


**Fig. 10** Grid convergence testing

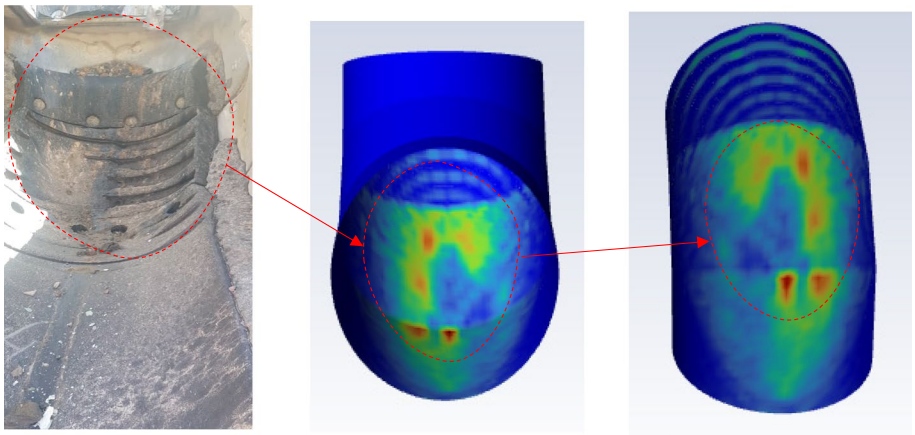

**Fig. 11** Comparison between the zone subject to strong erosion on the real chute and the simulated

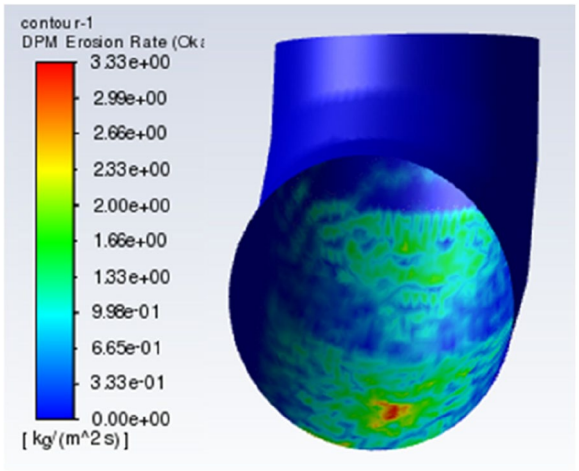


**Fig. 12** Erosion profile on rubber

the maximum density of the erosion rate remains constant, irrespective of the material employed. This stability is attributed to the unchanged impact area.

The main goals of this study were to anticipate erosion-prone areas along the chute, both qualitatively and quantitatively, with the aim of recommending a protective coating material that meets the company's specifications. Through a comparative analysis involving rubber, 316 stainless steel, and ceramic materials, the results, as depicted in Fig. 15, indicate that ceramic exhibits the highest resistance to erosion (0.6636753 kg/$m^2$s), outperforming 316 stainless steel (2.186633 kg/$m^2$s) and halogenated butyl rubber (3.326576 kg/$m^2$s).

The findings presented in this paper are corroborated by prior research indicating that ceramic coatings improve wear resistance and prolong the lifespan of mining equipment [2, 3]. Wolfe et al. [14] highlighted the fact that ceramic coatings provide a durable protective barrier for underlying substrates, surpassing many alternative film barrier materials such as polymers, metals, and glasses in terms of performance and effectiveness. Medvedovski [5] adds that ceramic coatings exhibit superior hardness compared to the particles

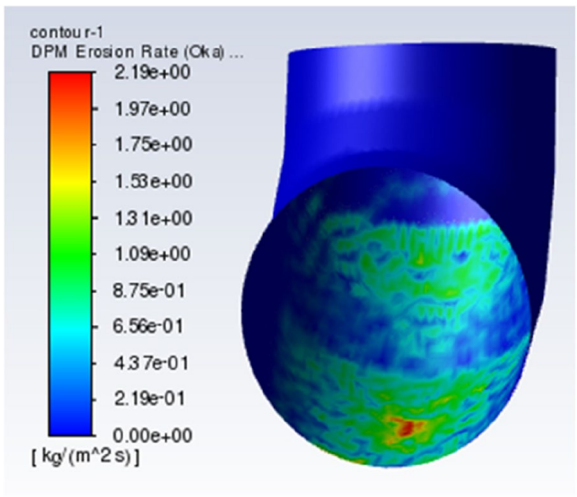


**Fig. 13** Erosion profile on 316 stainless steel

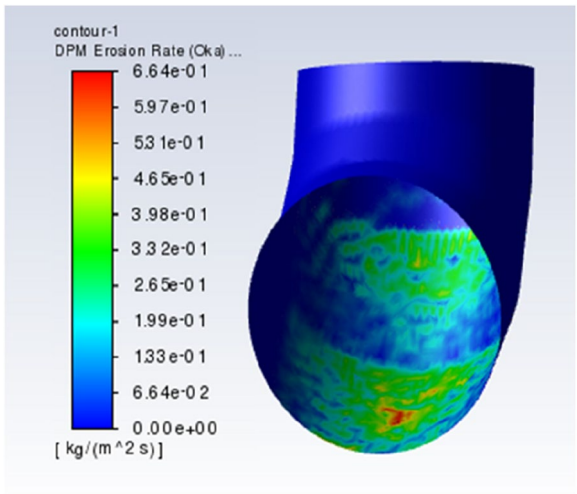


**Fig. 14** Erosion profile on ceramic

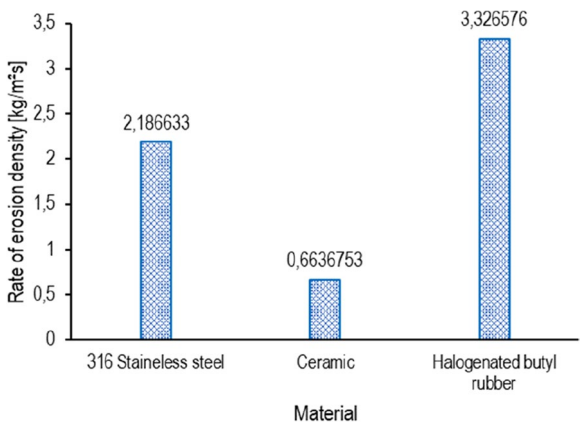


**Fig. 15** Comparison in terms of maximum erosion rate density

they encounter during processing, making them a preferred choice for wear applications in comparison to stainless steel protective skin. Additionally, the cracks that may form in ceramic coatings tend to be minimal due to the dominance of fracture toughness and brittleness, factors that contribute significantly to crack propagation and erosion resistance.

Given the findings above, both ceramic and steel show promise in potentially extending the average time between failures of the chute. Several solutions can be considered, including either a complete replacement of the protective coating or a localized replacement that targets the identified erosion-prone area. The choice between ceramic and 316 stainless steel should consider economic, financial, and technical factors. An alternative proposal involves combining halogenated butyl rubber with either ceramic or stainless steel. Halogenated butyl rubber, being elastic, offers shock absorption compared to the ductile and rigid nature of ceramic and 316 stainless steel. While ceramic and steel excel in abrasion resistance compared to rubber, a hybrid coating could merge the elasticity of rubber with the hardness of ceramic or 316 stainless steel, creating rubber-ceramic and/or rubber-stainless steel coatings.

For a rubber-ceramic coating, this could entail using rubber with recesses to house ceramic blocks, assembled with a high acid-resistant adhesive. Additionally, clamping holes could be strategically placed in erosion-resistant areas for bolting the new coating securely to the chute. Careful consideration of these options is crucial, considering the specific operational requirements and constraints of the mining environment.

Various methods and techniques are employed to apply different coating materials onto metal substrates, including physical vapor deposition, chemical vapor deposition, and thermal spraying [3]. The choice of a coating method typically depends on the specific application requirements and the characteristics of the substrate material. Each method yields distinct results in terms of raw material formulation, coating thickness, and density. Therefore, meticulous consideration of these factors is essential to achieve optimal mechanical strength and corrosion resistance [13].

## Conclusions

In conclusion, this study delved into the impact of different materials on the design of a protective coating for a crusher's feed chute. Utilizing computational fluid dynamics with Ansys Fluent, the research involved a thorough design and performance analysis of various protective coating materials, specifically examining erosion rates and density effects. Maximum densities for different materials were scrutinized, leading to the proposal of a new protective coating. The study observed the effects on the mean time between failures (MTBF) for feed chutes with different materials, highlighting the potential benefits of combining ceramic and steel or halogenated butyl rubber and ceramic to extend the chute's average time between failures. Through detailed modeling and simulations, the authors identified ceramic as a more favorable protective coating material, boasting a density rate of 0.6636753 kg/m$^2$s compared to 3.326576 kg/m$^2$s for halogenated butyl rubber and 2.186633 kg/m$^2$s for 316 stainless steel. The simulation results were derived from solid and liquid phase flow rates of 284.19 kg/s and 123.14 kg/s, respectively. This paper provides practical insights into the implications of the results through the lens of the authors' perspectives, demonstrating the significance of material choices in optimizing the protective coating for crusher feed chutes.

**Abbreviations**

| | |
|---|---|
| MTBF | Mean time between failures |
| CFD | Computational fluid dynamic |
| MMG | Minerals and Metals Group |
| SAG | Semi-autogenous grinding |
| RANS | Reynolds averaged Navier–Stokes |
| CAD | Computer-aided design |
| IGES | Initial Graphics Exchange Specification |
| STEP | Standard for the Exchange of Product Data |
| VOF | Volume of fluid |

**Acknowledgements**
Not applicable

**Authors' contributions**
Conceptualization: M.K. and L.T.; methodology: M.K., P.K., and L.T.; software: M.K. and P.K.; formal analysis: M.K., P.K., and L.T.; investigation: M.K.; writing—original draft preparation: M.K.; writing—review and editing: P.K., I.M., and L.T.; supervision: P.K and L.T.; project administration: L.T. All authors have read and agreed to the published version of the manuscript.

**Funding**
No funding was received to conduct the research.

**Availability of data and materials**
All data generated or analyzed during this study are disclosed within this published article.

## Declarations

**Competing interests**
The authors declare that they have no competing interests.

Received: 26 December 2023 Accepted: 9 May 2024
Published online: 18 May 2024

**References**

1. Ang C, Coste L, A Kerrien, Le Gac T, Neel C (2021) Modelisation des ecoulements Turbulents [Modeling of Turbulent Flows]. Moodle INSA Rouen. [Online] Available from https://moodle.insa-rouen.fr › Rapport_P6_2021_35. Accessed 15 Mar 2024
2. Chesterton. (2018) Protective coatings success stories for mining and ore processing equipment and structures. eBook available from: https://arcindustrialcoatings.chesterton.com/ArcDocuments/36586_Protective%20Coating_Mining_CS_eBook-FINAL.pdf. Accessed 15 Mar 2024
3. EPCM Holdings (n.d) Protective ceramic coatings in mining industry-materials & methods. [Online] Available from: https://epcmholdings.com/protective-ceramic-coatings-in-mining-industry-materials-methods/#:~:text=A%20ceramic%20coating%20extends%20the,repaired%20during%20scheduled%2C%20routine%20maintenance. Accessed 15 Mar 2024
4. Franklin JD (2009) An Eulerian/Lagrangian multiphase coupling algorithm for fluid particulate systems using arbitrary polyhedral mesh topologies. Wayne State University
5. Medvedovski E (2023) Advanced ceramics and coatings for erosion-related applications in mineral and oil and gas production: a technical review. Int J Appl Ceram Technol 20(2):612–659
6. Noguchi T (2010) Toward sustainable resource recycling in concrete society. Proceedings of the 2nd International Conference on Sustainable Construction Materials and Technologies, 321–334
7. Oka YI, Yoshida T (2005) Practical estimation of erosion damage caused by solid particle impact: Part 2: Mechanical properties of materials directly associated with erosion damage. Wear 259(1–6):102–109
8. Oka YI, Okamura K, Yoshida T (2005) Practical estimation of erosion damage caused by solid particle impact: Part 1: Effects of impact parameters on a predictive equation. Wear 259(1–6):95–101
9. Sánchez F, Hartlieb P (2020) Innovation in the mining industry: Technological trends and a case study of the challenges of disruptive innovation. Mining, Metallurgy & Exploration 37(5):1385–1399
10. Service Public de Wallonie (SPW) (2016) Fragmentation: Aide au choix d'équipements permettant la fragmentation de matières solides sur des bases énergétiques. Cahier technique No 19 Available from: https://energie.wallonie.be/fr/cahier-technique-sectoriel-la-fragmentation.html?IDC=8636&IDD=116958. Accessed 17 Sept 2023
11. Sellam R (2020) Analyse de Performance de Ventilation croisée à travers les grandes et les petites ouvertures ouvertures [Performance Analysis of Cross Ventilation Across Large and Small Apertures]. (Thèse de doctorat). Université de Sherbrooke, Sherbrooke, Canada
12. Suhr B, Skipper WA, Lewis R, Six K (2023) Sanded wheel-rail contacts: experiments on sand crushing behaviour. Lubricants 11(2):38
13. Thakare MR, Wharton JA, Wood RJK, Menger C (2007) Exposure effects of alkaline drilling fluid on the microscale abrasion–corrosion of WC-based hard metals. Wear 263(1–6):125–136

14. Wolfe DE, Ryan CJ, DeSalle CM, Stepanoff SP, Aronson BI, Boring ZM, Reiss JA, Albert PE, Nicastro JK, Fjeldsted AP (2023) A comprehensive review of modern engineered ceramics coatings for optimised resistance to wear and corrosion. Adv Appl Ceram 122(3–4):81–100
15. Xu Y, Li Z, Zhang G, Wang G, Zeng Z, Wang C, Wang C, Zhao S, Zhang Y, Ren T (2019) Electrochemical corrosion and anisotropic tribological properties of bioinspired hierarchical morphologies on Ti-6Al-4V fabricated by laser texturing. Tribol Int 134:352–364

## Publisher's Note